Effect of solution chemistry on the iodine release from iodoapatite in aqueous environments

Zelong Zhang [†,*], Léa Gustin[‡,1], Weiwei Xie[‡], Jie Lian[§], Kalliat T. Valsaraj[‖], and Jianwei Wang[†,⊥]

[†] Department of Geology and Geophysics, Louisiana State University, Baton Rouge, Louisiana 70803 United States

[‡] Department of Chemistry, Louisiana State University, Baton Rouge, Louisiana 70803 United States

[§] Department of Mechanical, Aerospace, and Nuclear Engineering, Rensselaer Polytechnic Institute, 110 Eighth Street, Troy, New York 12180, United States

[‖] Cain Department of Chemical Engineering, Louisiana State University, Baton Rouge, Louisiana 70803 United States

[⊥] Center for Computation and Technology, Louisiana State University, Baton Rouge, Louisiana 70803, United States

*Corresponding to zelongz@lsu.edu

[1] Current address: Department of Chemistry, University of Wisconsin-Madison, Madison, Wisconsin 53706, United States

Highlights

- First study on the effect of aqueous ions on the degradation of waste form for I-129
- First summary on probable iodine release pathways in various aqueous environments
- Accelerated iodine release by enhanced ion-exchange, basicity or acidity, and ionic strength
- Discovered secondary phase vanadinite $Pb_5(VO_4)_3Cl$ and hydroxylvanadinite $Pb_5(VO_4)_3OH$
- Low ionic content and neutral pH are vital to the disposal safety of nuclear waste

Abstract

To ensure the safe disposal of nuclear waste, understanding the release process of radionuclides retained in the nuclear waste forms is of vital importance. Iodoapatite $Pb_{9.85}(VO_4)_6I_{1.7}$, a potential waste form for iodine-129, was selected as a model system for ceramic waste forms in this study to understand the effect of aqueous species on iodine release. Semi-dynamic leaching tests were conducted on bulk samples in cap-sealed Teflon vessels with 0.1 mol/L NaCl, Na_2CO_3, Na_3PO_4, and Na_2SO_4 solutions under 90 °C, fixed sample surface area to solution volume ratio of 5/m, and periodic replacement of leaching solutions. The reacted solutions were then analyzed by Inductively Coupled Plasma-Mass Spectrometry and Inductively Coupled Plasma-Optical Emission Spectrometry; the leached surfaces were characterized by X-ray diffraction, scanning electron microscopy, and infrared spectroscopy. The result shows that, compared to deionized water, the ion-rich solutions enhanced the iodine release as a result of the increased ionic strength, reduced activity coefficient of dissolved species, and increased solution pH. Surface reactions can lead to the formations of secondary phases by ion-exchange and precipitation. These findings suggest that an ion-rich environment in the geological repository can be detrimental to the disposal safety of the nuclear waste form.

1 Introduction

Nuclear energy is emission-free. The deployment of nuclear energy is motivated by the pressing demand to mitigate climate change.[1] Sustainable development of the nuclear energy requires concrete plans to safely dispose radionuclides waste generated by nuclear fission.[2] Among those radionuclides, iodine-129 is particularly challenging to handle due to its long half-life (15.7 million years), high yield (0.7% yield per fission of uranium-235),[3] and weak interactions with common materials in repository environments such as engineering barrier and rock in geology formation.[4,5] Iodide (I^-) is the most stable form of iodine in an environment with pH and redox potential typically found in nature.[6–8] Under highly oxidizing conditions, iodide can be oxidized to iodine (I_2) and/or iodate (IO_3^-). All these iodine species are highly mobile in nature given their high volatility and or high solubility.[9,10] Iodine, as an essential element for human health, can accumulate in human bodies.[11] For a healthy adult, 30% of the total iodine, approximately 15-20 mg, is concentrated in the thyroid gland.[12] Chronical radiation from iodine-129 beta decay can induce cancer to the thyroid follicular cells.[11] Therefore, iodine-129 is a primary contributor of the radiation dosage when analyzing the safety of disposal environments.[4] The immobilization of iodine-129 is one of the critical research subjects for nuclear waste management.[4,13–18]

The most probable scenarios that compromise nuclear waste forms in a repository environment are the contact with aqueous solutions.[19,20] In a typical repository, nuclear waste forms are packed into corrosion resistant metallic canisters underground.[21] Canister corrosion and degradation are anticipated to be the result of corrodents carried by groundwater.[22] Through infiltration and percolation of precipitation and groundwater aquifer, water can reach the canisters and supply corrodents to react with the canister material. Upon the breaching of the

canister, the waste forms are exposed to an aqueous environment. Owing to the long half-life of iodine-129, it is crucial to predict the long-term chemical durability of iodine waste forms. To enable such prediction, it is necessary to obtain a fundamental understanding of corrosion mechanisms of waste forms and how iodine in the host material is released in various solutions that may occur under repository conditions.

Several waste form materials including glass, ceramics, glass-ceramics, cement, and composite have been proposed to immobilize iodine.[18,23] These waste forms immobilize iodine via two major mechanisms: encapsulation and incorporation. To encapsulate iodine, the host matrices need to contain iodine in a designated phase different from the host material. One example is zeolite structure, in which iodine-bearing phases can be adsorbed on zeolite's framework.[17,24] Iodine can also be incorporated as a compositional element into the host matrix structure through chemical bonding, such as iodoapatite $Pb_5(VO_4)_3I$ and sodalite $Na_4(AlSiO_4)_3I$.[13,25–27]

The difficulty to study the durability of different waste forms varies on a case-by-case basis. It is particularly challenging to evaluate the encapsulation waste forms due to the complexity of multi-phase and microstructures. On the other hand, characterizing the corrosion mechanism can be relatively straightforward for single-phase crystal waste forms which have well-defined crystal structures and simple microstructures. Based on the simplicity of its crystal structure and microstructure, iodoapatite is chosen in this study as the model system of ceramic waste forms that can incorporate radionuclides. In addition, apatite ceramics is a promising material due to its thermal, mechanical, and chemical stability.[13,25,28,29] These advantages are also demonstrated in nature as apatite has been found as a retention matrix for actinides and fission products in natural fission reactors at Franceville basin in Africa.[22,30]

Several chemical durability tests have been performed on single-phase crystal waste forms. Uno et al. in 2001 conducted soxhlet leach method on apatite $Pb_{10}(VO_4)_6I_2$.[31] Soxhlet leach method is designed to maximize the number of leachable constituents in leachant by allowing a continuous contact between the waste and recycling leachant in a closed system.[32] The iodine release rate, 3.98×10^{-5} $g\cdot cm^{-2}\cdot d^{-1}$, was reported.[31] Guy et al. in 2002 studied apatite $Pb_{10}(VO_4)_{4.8}(PO_4)_{1.2}I_2$ dissolution in aqueous solutions.[33] The resulting data shows that iodine release was incongruent and exhibited dependency on temperature and pH. They also discovered a secondary phase, lead vanado-phosphate, precipitated at the sample surface. Zhang et al. in 2007 performed static leaching test on $Pb_5(VO_4)_3I$ powder in a basic $KOH/KHCO_3$ buffer solution.[34] Spectroscopic evidences show that OH^- and CO_3^{2-} can substitute I^- and VO_4^{3-} in apatite. Maddrell et al. in 2014 conducted static leach tests on crushed powder iodide sodalite $Na_4(AlSiO_4)_3I$ in $KOH/KHCO_3$ buffer solutions.[26] The result suggests a congruent dissolution.[26] Three leaching static experiments with durations of 3, 7, and 14 days exhibited a logarithmic increase of iodine release. More recently, in 2017 Coulon et al. applied static leaching technique to study the iodate-substituted hydroxyapatite in deionized water and groundwater.[35] They reported that the iodine release is controlled by congruent dissolution under unsaturated conditions and controlled by diffusion through ion exchange under saturated condition. Interestingly, when groundwater was used as leachant, secondary phase hydroxyapatite precipitated on the sample surface. Based on these studies, static leach test is a preferable method to study the waste form durability due to the following reasons: 1) its simple procedure can accommodate a wide range of test conditions; 2) the resultant data can be used to interpret the release mechanism.[36] Static leaching method assumes that the solution feedback is negligible, which is valid under conditions of sufficiently low surface to volume ratio.[36] However, the

109 solution feedback can gradually increase over time in a static leaching experiment. In cases
110 where the solution is oversaturated for phases of low solubility, secondary phases can precipitate
111 at the leached surface. Therefore, it can be problematic to use data from static leaching tests to
112 predict waste form behavior in a repository environment.[37] To address the issues of solution
113 feedback, a semi-dynamic leaching method was implemented by Zhang et al. in 2018 to quantify
114 the processes involved in the iodine release of an iodine-bearing apatite.[29] In their experiment,
115 deionized water solutions, as the leachant, were replaced periodically to minimize the solution
116 feedback. They demonstrated that iodine released from apatite is driven by short-term diffusion
117 and long-term matrix dissolution. This semi-dynamic approach was employed to produce
118 essential datasets to parameterize a mechanistic model suitable for predicting the kinetics of
119 iodine release under different conditions.[37]

120 Since the aqueous systems in natural environment contain a variety of dissolved species, it is
121 necessary to understand how these aqueous species affect the iodine release from iodine waste
122 forms in an aqueous environment. For instance, the iodine release from apatite structured
123 materials can be enhanced by rapid substitution of halogen element[38–41] or inhibited by
124 precipitation of secondary phase.[33,35,37] In this study, we conducted semi-dynamic leach tests on
125 single phase crystal ceramics of iodoapatite in 0.1 mol/L NaCl, Na_2CO_3, Na_3PO_4 and Na_2SO_4
126 solutions. The goal is to examine the impact of the solution chemistry on the kinetics of
127 iodoapatite dissolution. We hypothesized that dissolved aqueous species, via ion exchange and
128 precipitation, can substantially impact the dissolution kinetics; this effect should highly depend
129 on the chemistry of the aqueous species and the surface reactions of specific phases. The finding
130 of this study is expected to provide important insight into the long-term performance of iodine
131 waste forms and guidance to improve the disposal safety of nuclear waste.

2 Experimental

2.1 Materials and methods

Our samples, obtained from previous studies,[25] were dense ceramic chips in quadrilateral shape: 4.7 – 10.3 millimeter long by 1.1 – 1.8 millimeter thick with a chemical composition of $Pb_{9.85}(VO_4)_6I_{1.7}$ according to the EDS and X-ray diffraction refinement, as shown in Figs. 1, 2 and 4. The iodoapatite samples were synthesized by using high energy ball milling (HEBM) and spark plasma sintering (SPS) techniques. Sample surfaces were polished by 4000-grit sandpaper on a mechanical polishing wheel lubricated with ethanol. Details of the synthesis and characterization of these samples were reported previously in separate publications.[25,29,37]

The leaching method was adopted from ASTM C1308 standard test, as described in the previous study[29,37]. Four parallel experiments were conducted simultaneously for 14 days in four different leaching solutions: 0.1 mol/L NaCl, 0.1 mol/L Na_2CO_3, 0.1 mol/L Na_3PO_4, and 0.1 mol/L Na_2SO_4. Sample surface area (m^2) to solution volume (m^3) ratios (S/V) of all four tests were fixed and maintained at 5/m. The leached solutions were replaced every 24 hours. All reactor vessels were weighed before and after each interval to monitor the solution losses which were within 0.5 % of the initial solution mass. In addition, a control test was conducted in deionized water under identical conditions for 7 days using the same protocol. All samples after leaching experiments were collected, rinsed by deionized water and ethanol, and air-dried.

2.2 Characterization

153 The elements of interest in the leachate solutions are I, Pb, and V. The leached
154 solutions, depending on the solution chemistry, were analyzed by Inductively Coupled
155 Plasma-Mass Spectrometry (ICP-MS, PerkinElmer Elan 9000) and/or Inductively-
156 Coupled Plasma-Optical Emission Spectrometry (ICP-OES, SPECTRO Ametek Spectro
157 ARCOS). Two standard solutions from Inorganic Ventures were used in the solution
158 analysis: 1) 1.001 ± 0.007 μg/ mL iodide in H_2O solution and 2) 1.000 ± 0.007 μg/ mL
159 lead and 1.000 ± 0.006 μg/ mL vanadium in 1% HNO_3 solution. Chemical properties of
160 solution at equilibrium state such as pH, ionic strength, speciation, and activity were
161 calculated by Visual MINTEQ package.

162 Samples were characterized by Scanning Electron Microscopy (SEM), Infrared
163 spectroscopy (IR), and X-ray diffraction spectroscopy (XRD). SEM images were taken by
164 a FEI Quanta SEM system with FEI Versa 3D DualBeam. Infrared spectroscopy was
165 performed on a Thermo Nicolet Continuum Infrared Microscope under Specular
166 Reflection mode and transmission mode with a fixed incident angle and an aperture area
167 of 10 by 10 μm covering 4000 to 650 cm^{-1} at a spectral resolution of 2 cm^{-1}. XRD data
168 were collected from PANalytical Empyrean X-Ray Diffractometer equipped with
169 monochromated Cu-Kα radiation (λ = 1.5406 Å), operated at 45 kV, 40 mA, a step size of
170 0.026°, and a scanning range from 5 to 100°.

171 The crystal structures were refined by Le Bail algorithm using Jana2006 program.[42]
172 All parameters were refined by the least-squares method. The pseudo-Voigt function was
173 used as the peak profile function. Structural parameters of $Pb_{9.85}(VO_4)_6I_{1.7}$ measured by
174 Audubert et al. were used as initial input (hexagonal, space group P63/m, a = b = 10.422
175 Å, c = 7.467 Å, α = β = 90°; γ = 120°).[43]

3 Results

3.1 Leached surface characterization by SEM/EDS

In Fig. 1 (a-c), no changes observable by naked eyes occurred on the surfaces of samples leached by NaCl and $NaSO_4$ solutions for 14 days, whereas white layers were gradually formed on the sample surfaces leached by Na_2CO_3 and Na_3PO_4 solutions within the first week of the experiments. The SEM images in Fig. 1 (d-i) show that the surface alterations on samples leached by NaCl and Na_2SO_4 solutions were moderate, similar to the water leached surface. However, samples leached by Na_2CO_3 and Na_3PO_4 solutions demonstrated significant surface corrosion and possible formation of new phases. The surface leached by Na_2CO_3 exhibited large grains, while congregated structures of similar size appeared on the surface leached by Na_3PO_4.

According to EDS analysis, the surface chemical compositions in Fig. 2 indicate considerable changes between the leached samples and the pristine one. The key features of EDS spectrum of pristine iodoapatite are: a carbon peak at 0.3 keV from background (carbon tape), an oxygen peak at 0.5 keV, a broad Pb band from 2.34 to 2.45 keV shouldered with two small Pb peaks at 1.8 and 2.6 keV, three iodine peaks at 3.9, 4.2, and 4.5 keV, and vanadium peaks at 4.9 and 5.4 keV. Overall, the iodine peaks at 3.94 keV are nearly diminished in the EDS spectra of all four leached surfaces. The samples leached by NaCl and Na_3PO_4 exhibited a substantial amount of chloride and phosphorus signals at 2.62 and 2.01 keV, respectively. On the sample leached by NaCl, the Pb peak at 2.62 keV is comparable to the Pb peak at 1.8 keV, while the 2.62 keV peaks of the rest samples are much weaker than their corresponding 1.8 keV peaks. Carbon signal at 0.27

198 keV from Na_2CO_3 leached sample cannot be properly quantified due to the background
199 interference from carbon tape and the graphite impurity introduced during sample
200 synthesis. Sulfur EDS peak at 2.31 keV overlaps with the broad central peak of Pb at 2.34
201 keV. Na_2SO_4 leached surface exhibited no sulfur peak near 2.3 keV given the
202 resemblance of the band shape between the sample leached by Na_2SO_4 and the rest. We
203 noticed variations of carbon and oxygen EDS signals among these samples which were
204 induced by the instrumentation settings such as sample orientation and beam parameters.
205 Therefore, carbon and oxygen were not considered in the EDS analysis.

206 **3.2 Leached surface characterization by IR analysis**

207 The IR spectroscopy results are listed in Fig. 3. All these four samples yielded two
208 main peaks near 750 and 890 cm^{-1}, which are attributed to V-O bond.[34] Pristine
209 iodoapatite and samples leached by water, Na_2SO_4, and NaCl showed nearly identical
210 spectra. Surfaces leached by Na_2CO_3 and Na_3PO_4 exhibited position shifts of these two
211 V-O peaks to the region of 700 to 900 cm^{-1} and multiple new bands. Sample leached by
212 Na_2CO_3 yielded sharp bands near 785, 890, 960, 1200, and 1450 cm^{-1}, in which the broad
213 band at 1450 cm^{-1} is attributed to the stretching vibration of CO_3^{2-}.[44,45] The Na_3PO_4
214 leached surface generated IR peaks near 785, 870, 950, 1110, 1420, 1800, and 2200 cm^{-1},
215 in which some can be assigned to the PO_4^{3-} (e.g. ν_1 – 950 cm^{-1}, ν_3 – 1100 cm^{-1}).[44]
216 Interestingly, both CO_3^{2-} and PO_4^{3-} leached surfaces showed visible OH^- stretching
217 vibration near 3500 cm^{-1},[34,44] which also occurred on water leached surface under IR
218 transmission mode.[29]

219 **3.3 Leached surface characterization by XRD**

The XRD data are shown in Fig. 4. All these leached samples demonstrated substantial differences compared to the pristine sample. Based on the XRD pattern, these leached samples can be categorized into two groups: I) surfaces leached by NaCl and Na_2SO_4 solutions, the pristine, and water leached sample; II) surfaces leached by Na_2CO_3 and Na_3PO_4 solutions, which were similar to the standard hydroxylvanadinite. The XRD patterns of Group I are alike, which indicates no substantial structural changes compared to the pristine. The XRD patterns of Group II display enhanced peak splitting between 25° and 28°. The original peak splitting of the pristine sample reflects the apatite structure deformation which accommodates the relatively large iodide incorporated in the apatite framework. The peak splitting of Na_2SO_4 leached surface is slightly enhanced, compared to the pristine, but is weaker than the water leached sample. Interestingly, NaCl leached surface yielded a diminished splitting at 26° and a new peak occurred at 29°, later identified as $1\bar{3}1$ shown in Fig. 5. The Full Width at Half Maximum (FWHM) of XRD from NaCl leached surface was considerably broadened to ~0.4° compared to ~0.2° from other samples, which may be attributed to the peak overlapping resulting from the presence of a secondary phase. Both Na_2CO_3 and Na_3PO_4 leached samples exhibited nearly identical XRD pattern, resembling the pattern of standard hydroxylvanadinite $Pb_{10}(VO_4)_6(OH)_2$. The two highest bands on $Pb_{10}(VO_4)_6(OH)_2$ standard are 112 and $1\bar{3}1$ with an order of intensity $I_{112} < I_{1\bar{3}1}$. Same bands 112 and $1\bar{3}1$ also have the highest intensity on Na_2CO_3 and Na_3PO_4 leached samples, however, the intensity of 112 is higher than that of $1\bar{3}1$, $I_{112} > I_{1\bar{3}1}$.

The Le Bail method was applied to obtain structural information from the XRD data. Table 1 compares the refined lattice parameters between sample surfaces of different

conditions and standards. No noticeable changes occurred in the crystal structures of samples leached by deionized water and Na_2SO_4 when compared to that of pristine sample (their length of *a*-, *b*-, and *c-axes* are approximately ~10.4, ~10.4, and ~7.5 Å, respectively). On the other hand, a ~0.2 Å contraction along both the *a*- and *b*-axes were observed for the samples leached by Na_2CO_3 and Na_3PO_4 solutions while the *c*-axis remains the same and is consistent with other samples at ~7.45 Å. The observed and calculated diffraction patterns, the residual and the indices of the main reflections of NaCl leached sample are shown in Fig. 5. We identified a secondary phase vanadinite $Pb_5(VO_4)_3Cl$, indicating the substitution of iodine by chlorine during NaCl leaching.

3.4 Solution composition analysis by ICP-MS and ICP-OES

The results of the solution analysis on the leachates collected from the leach tests are shown in Fig. 6. The release rates of iodine, lead, and vanadium are depicted as green circles, blue squares, and red triangles, respectively. In Fig. 6(a), iodine release in NaCl solution gradually increased over time, reaching a maximum rate near 0.8 mmol/m^2/d at day 11, and then slightly decreased near the end of the 14-day test. The Pb and V release exhibited similar patterns with a relatively high initial rate around 0.075 mmol/m^2/d, then gradually decreased, and eventually approached a plateau near 0.05 mmol/m^2/d. In Fig. 6(b), the release patterns of iodine and vanadium in Na_2CO_3 are similar: release rates rapidly reached maximum near day 2 and then gradually decreased over time approaching a plateau. However, the long-term rate of Pb in Na_2CO_3 appears to be constant. In Fig. 6(c), the iodine release in Na_2SO_4 exhibited a high initial rate approximately 0.32 mmol/m^2/d and then its rate gradually decreased, eventually approaching a plateau around 0.15 mmol/m^2/d. Despite no high initial release, the Pb and V release patterns follow the

trend of iodine release: gradually decreased over time and then rebounded near day 10. The Fig. 6(d) describes the element release of iodoapatite in Na_3PO_4, which shows constant rates of ~4.5, ~3.5, and ~13 mmol/m^2/d for the release for iodine, Pb, and V, respectively. Due to the instrumentation limitation and sample consumption, only four leachates from the Na_3PO_4 experiment was analyzed for their Pb content.

Leaching rates of I, Pb, and V based on the solutions analysis are compared in Figs. 7(a-c), respectively. In general, leaching tests conducted in the ionic solutions present significantly higher element release rates than those of deionized water in the order of Na_3PO_4 > Na_2CO_3 > Na_2SO_4 > water, except in the NaCl solution. In Fig. 7(a), iodine release from Na_3PO_4, Na_2CO_3, and Na_2SO_4 solutions exhibited a long-term leach pattern similar to that of water leaching: started with a high initial release, then gradually decreased, and eventually stabilized and reached a plateau. The iodine release in NaCl solution, however, presents a different pattern: iodine rate increased from the beginning of leach test to day 11, when the rate reached maximum and then stabilized. The release rates of Pb and V from NaCl test are relatively constant but not higher than those of water leached as shown in Figs. 7(b, c).

The molar ratios in leachate solutions are illustrated in Figs. 7(d, e). Except for the anomalous NaCl data, the long-term I/V ratios in Fig. 7(d) fluctuate around the ratio of water-leached sample within the range of [0.34, 1.02], which are higher than the stoichiometric value 0.28. In Fig. 7(e), the long-term Pb/V ratios of NaCl and Na_2SO_4 tests are 1.36 and 1.65, approximate to the stoichiometric value 1.64, whereas the long-term ratios from Na_2CO_3 and Na_3PO_4 tests are 0.95 and 0.27, significantly lower than 1.64.

3.5 Overview of leaching rates in solutions

The phases of interest in this study are the aqueous solutions and the solid surfaces. The leachate solution chemistry in Fig. 7 shows that iodine release from the sample leached by the NaCl solution has a distinctive pattern. For the other leach tests, the long-term iodine rates (plateau region in Figs. 6-7) are at least one magnitude higher than that from water leaching. And the order of iodine leach rate, based on solution analysis in Fig 7 (a), is consistent with the orders of Pb and V rates in Fig. 7 (b, c): $R_{Pb/V/I}$ (Na_3PO_4) > $R_{Pb/V/I}$ (Na_2CO_3) > $R_{Pb/V/I}$(Na_2SO_4) > $R_{Pb/V/I}$ (deionized water). In the following section, we will analyze the anomalous result of NaCl leach test and then explain how element release behaviors differentiate due to the different solution chemistry, such as pH and ionic species.

4 Discussion

4.1 Anomaly of the sample leached by NaCl solution

Iodoapatite sample leached by 0.1 mol/L NaCl solution exhibited unique surface phase composition and iodine release pattern. The XRD data in Figs. 4 and 5 show leached surface has no apparent splitting in the region from 25° to 28° (2θ) and a new peak $(1\bar{3}1)$, attributed by a vanadinite phase. This anomaly suggests a reduced structural distortion, which can be contributed by substituting iodide with smaller chloride. The refinement in Fig. 5 confirmed new phase vanadinite was formed on the surface, which resembles the XRD pattern of iodoapatite $Pb_{9.85}(VO_4)_6I_{1.7}$. The XRD data is consistent with the EDS result and solution analysis. The Pb EDS band at 2.6 keV, in Fig 2, is comparatively enhanced due to the overlap by chlorine signal at 2.6 keV. The release

311 rates of iodine from the NaCl test in Fig. 6(a) suggest the new phase was growing until
312 the equilibrium state was reached. A similar iodine release pattern was observed in a pH 4
313 semi-dynamic leaching experiment, of which the rate anomaly was caused by the
314 formation of a secondary phase.[37] The molar ratios of Pb/V in Fig. 7(e) approximate to
315 the stoichiometric value 1.6, indicating a congruent dissolution of Pb and V. The variation
316 of I/V molar ratios in Fig. 7(d) is consistent with that of iodine rates in Fig. 6(a). Both the
317 I/V ratios and iodine rates suggest an incongruent release for iodine, unlike the congruent
318 Pb and V. The SEM images in Figs. 1(b, e) show that both surfaces leached by NaCl and
319 deionized water share similar morphology. The new phase vanadinite $Pb_5(VO_4)_3Cl$,
320 confirmed by the XRD refinement, suggests ion-exchange process between iodide and
321 chloride. This postulation is supported by the solution and surface analysis that 1) a
322 significant amount of iodine was released into NaCl solution while the Pb and V rates are
323 comparable to the data of water leach test as shown in Figs. 6-7; 2) the surface alteration
324 revealed by SEM in Fig. 1 and the surface chemistry by EDS in Fig. 2 resemble those of
325 deionized water. Interestingly, the structural deformation of the original iodine-bearing
326 apatite $Pb_{9.85}(VO_4)_6I_{1.7}$ appeared to be restored in the chlorine-substituted structure
327 vanadinite $Pb_5(VO_4)_3Cl$. Given that the ionic radius of chloride (Cl^-, 1.68 ± 0.19 Å) is
328 considerably smaller than that of iodide (I^-, 2.11 ± 0.19 Å),[46] exchanging the iodide with
329 smaller chloride seems to have repaired the structural deformation.

330 **4.2 Effect of pH on iodine release and secondary phase formation**

331 The solution pH has a strong effect on the iodine release of the iodoapatite. Chemical
332 properties of the leaching solutions calculated by VMINTEQ are listed in Table 2.
333 According to our previous studies, iodoapatite dissolution in deionized water can be

represented by the congruent release of Pb and V.[29] In Fig. 7 (b, c), the Pb and V rates from different solutions are generally constant, indicating a constant-dissolution controlled process. The overall dissolution rates from low to high appears to be: *R (deionized water)* < *R* (Na_2SO_4) < *R* (Na_2CO_3) < *R* (Na_3PO_4), which corresponds to the solution pH values ~6.1, ~6.2, ~10.3, and ~10.9 under 90 °C as listed in Table 2. Therefore, increasing pH from neutral to basic can increase the iodine release by enhancing the overall dissolution of the iodoapatite, which is consistent with previous experimental results on synthetic iodoapatite and natural apatites[33,47]. However, due to the secondary phase formed in Na_2CO_3 solutions, the dissolution process was being continuously hindered by the accumulating precipitates. Interestingly, the trend of iodine released in Na_2CO_3 solution of pH 10.3 resembles that of leaching iodoapatite under pH 4.[37] Despite the rate difference, both surfaces leached by pH 4 and pH 10.3 formed secondary phases (chervetite and hydroxylvanadinite, respectively). Our previous study showed that the equivalent long-term rate of iodine release under pH 6 is 8.1 mmol/m^2/d, over two magnitudes higher than that of the deionized water 0.036 mmol/m^2/d.[37] Nevertheless, the release rates of iodine leached by the solutions of non-neutral pH are at least one magnitude higher than that of the neutral pH solutions due to the enhanced dissolution process.

Surface characterizations indicate the presence of new phases under the basic conditions. The XRD analysis in Fig. 4 and Table 1 shows the surfaces leached by the Na_2CO_3 and Na_3PO_4 solutions were dominated by secondary phases resembling hydroxylvanadinite $Pb_{10}(VO_4)_6(OH)_2$. The SEM in Fig. 1 reveals different grain shapes and sizes from the water leached, while the EDS in Fig. 2 demonstrates that iodine was

depleted on the surface. The solution analysis also supports the formation of new phase given the similar element release pattern to that of pH 4 and incongruent Pb/V ratios far away from the stoichiometric value. As shown in Fig. 7, the leaching rates of all elements are at least one magnitude higher than the water leach rates of corresponding elements. The results from this study and those from relevant literature suggest that the solution pH exerts significant effects on the dissolution rate and the secondary phase formation in aqueous environments such as chervetite and hydroxyvanadinite precipitated under acidic and basic conditions, respectively.[37,48,49]

4.3 Effect of ionic species on the dissolution rate

In this study, dissolved species affected the sample dissolution process by increasing the ionic strength in solution, which consequently reduced the activity coefficient of dissolved species. As a result, saturation state and solution feedback were reduced, which in return increased the dissolution rate.[47] Although the 0.1 mol/L Na_2SO_4 and 0.1 mol/L NaCl solutions have approximately the same solution pH as deionized water, the dissolution rates in these ionic solutions are significantly higher than that of the deionized water. As shown in Table 2, 0.1 mol/L Na_2SO_4 solution gives total ionic strength of 0.26 mol/L, 0.1 mol/L NaCl solution 0.098 mol/L, and deionized water 2.04×10^{-6} mol/L close to zero. The vast difference in ionic strength leads to different degrees of saturation state. The activity coefficient of the major ions Na^+, Cl^-, and SO_4^{2-} in these ionic solutions are ranging from 0.25 to 0.76, considerably lower than the major ions H^+ and OH^- with a respective activity coefficient 1.00 in the deionized water. The dissolution rate in 0.1 mol/L Na_2SO_4 solution is higher than the rate in the 0.1 mol/L NaCl solution and deionized water under the same pH and reaction mechanism, as shown in Fig. 7.

Moreover, the average release rate of iodine in Na_3PO_4 (pH 10.9) is about one magnitude higher that of Na_2CO_3 (pH 10.3) despite their similar pHs. The difference in rates can be inferred from the difference in ionic strength: 0.29 mol/L for 0.1 mol/L Na_3PO_4 and 0.25 mol/L for Na_2CO_3 solution.

In addition, no substantial structure change happened to the sample leached by 0.1 mol/L Na_2SO_4 solution. It is unlikely that anion SO_4^{2-} can be incorporated into apatite structure as there is no evidence from surface characterization and solution analysis to support that. No structural change was detected by the XRD characterization. The SEM images and EDS analysis in Figs. 1 and 2 show that the Na_2SO_4 and water leached surfaces have a similar grain size, surface morphology, and chemical composition. The element release rates and ratios in Fig. 7 and 8 demonstrate a similar leach behavior between samples leached by Na_2SO_4 and deionized water. The similarities in surface alteration and leaching behavior between samples leached by Na_2SO_4 and water suggest that the iodine release in Na_2SO_4 solution was controlled by short-term diffusion and long-term dissolution and the release of Pb and V is controlled by congruent dissolution. No precipitated was observed on Na_2SO_4 leached surface, which is also similar to the surface leached by water.

In terms of the surface precipitation, the SEM images in Figs. 1 (c, f) reflect intense surface alterations in the solutions of Na_3PO_4 and Na_2CO_3. The leached surfaces yielded XRD patterns similar to the standard hydroxyvanadinite $Pb_5(VO_4)_3OH$. However, significant contractions of *a*- and *b*-axes as shown in Table 2 indicate the size of VO_4 site was reduced, which could be caused by a substitution of smaller groups.[50] The IR spectroscopy of the sample leached by Na_3PO_4 confirms the existence of P-O bond and

OH^-. Furthermore, the EDS detected phosphorus signal, which also supports that PO_4 group was in VO_4 site. The molar ratios of Pb/V in Fig. 7 show a deficiency of Pb relative to V in Na_3PO_4 leaching test. These evidences suggest the precipitates are a product of hydroxyvanadinite with mixed site: $Pb_{10}(VO_4)_n(PO_4)_{6-n}(OH)_2$. The site mixing is possible since $Pb_{10}(VO_4)_x(PO_4)_{6-x}(OH)_2$ can occur during wet chemistry reactions under similar conditions.[48] Carbonate is known to be incorporated into apatite structure by substitution.[50–53] Given that phosphate (PO_4^{3-}, ionic radius 2.30 ± 0.42 Å)[46] can replace vanadate in iodoapatite,[48] it is reasonable to presume that carbonate of a smaller ionic radius (CO_3^{2-}, 1.89 ± 0.19 Å)[46] can substitute vanadate in a similar crystal structure. Therefore, the secondary phase formed on in the Na_2CO_3 solution is $Pb_{10}(VO_4)_{6-m}(CO_3)_{1.5m}(OH)_2$.

4.4 Mechanism of iodoapatite dissolution and surface reactions in aqueous environments

Fig. 8 generalizes the mechanism of iodoapatite dissolutions with multiple processes contributing to the iodine release. Our previous study on iodine release in deionized water suggests that the iodine release is driven by short-term diffusion and long-term dissolution.[29] Diffusion and dissolution are affected by various factors of the solution chemistry, such as solution ionic strength, pH, and secondary phase formation resulted from a supersaturation of the solution with respect to low solubility species. In neutral pH solutions, the iodine release is subjected to the substitution of iodine by anionic species in solution such as OH^- and Cl^-. When dealing with solutions of comparable pH, a higher ionic strength, due to the ionic content, can enhance the dissolution by changing saturation conditions. Solution pH other than near neutral can increase the dissolution by

exponentially accelerating the dissolution process. The resulting rapid dissolution can often lead to the precipitation of secondary phases when the solution approaches the supersaturation state of low solubility phases. Possible secondary phases include chervetite $Pb_2V_2O_7$ under acidic condition[37] and hydroxylvanadinite $Pb_5(VO_4)_3OH$ under basic condition.

5 Conclusions

The present study focuses on effects by solution compositions on iodoapatite dissolution. The results suggest that the higher ionic strength can accelerate dissolution by decreasing the activity coefficient of reacting aqueous species, thus promoting iodine release from apatite. Non-neutral pH conditions clearly increase the dissolution rate and often lead to precipitations of secondary phases, such as chervetite and hydroxylvanadinite. The secondary phase precipitation at the surfaces hinders the dissolution rate by reducing the available reacting surface area. However, the overall iodine release rates in both basic and acidic solutions are exponentially higher than those in the near-neutral pH conditions, especially in deionized water. Current understanding of dissolution is mostly based on leaching experiments conducted in deionized water. Our investigation on the impact of solution chemistry reveals new complexities of the dissolution kinetics of crystalline waste form during environmental degradation, Unlike fresh water with low ion content, high concentrations of aqueous species commonly found in underground brines can compromise the chemical durability of crystalline waste form in a geological repository. For this specific waste form, maintaining neutral pH and low ion content in aqueous solutions is important to the disposal safety of radioactive iodine. Since iodine is one of the most challenging radionuclides to immobilize, building

449 a comprehensive theoretical framework of iodine immobilization can significantly
450 advance the research in nuclear waste disposal safety.

451 Conflicts of interest

452 There are no conflicts to declare.

453 Acknowledgements

454 This work was supported as part of the Center for Performance and Design of Nuclear
455 Waste Forms and Containers, an Energy Frontier Research Center funded by the U.S.
456 Department of Energy, Office of Science, Basic Energy Sciences (DE-SC0016584). The
457 sample surface characterizations were carried out at the Shared Instrumentation Facilities
458 (SIF) and Center for Advanced Microstructures and Devices (CAMD) of Louisiana State
459 University. We thank our XRD & Geochemistry Lab Researcher Wanda LeBlanc for
460 operating XRD experiments at SIF and facilitating our experiments in Geochemistry Lab.
461 We also thank Dr. Orhan Kizilkaya from CAMD for his assistance on infrared
462 spectroscopy.

463 Date Availability

464 Data will be made available on request

References

(1) Climate Change 2014: Mitigation of Climate Change: Working Group III Contribution to the Fifth Assessment Report of the Intergovernmental Panel on Climate Change; Intergovernmental Panel on Climate Change, Edenhofer, O., Eds.; Cambridge University Press: New York, NY, 2014.

(2) Alley, W. M.; Alley, R. The Growing Problem of Stranded Used Nuclear Fuel. Environ. Sci. Technol. **2014**, 48 (4), 2091–2096. https://doi.org/10.1021/es405114h.

(3) Nichols, A. L.; Verpelli, M.; Aldama, D. L. Handbook of Nuclear Data for Safeguards; INDC(NDS)--0502; International Atomic Energy Agency, 2007.

(4) Ojovan, M. I.; Lee, W. E. 10 - Long-Lived Waste Radionuclides. In An Introduction to Nuclear Waste Immobilisation (Second Edition); Ojovan, M. I., Lee, W. E., Eds.; Elsevier: Oxford, 2014; pp 107–115. https://doi.org/10.1016/B978-0-08-099392-8.00010-3.

(5) Aimoz, L.; Wieland, E.; Taviot-Guého, C.; Dähn, R.; Vespa, M.; Churakov, S. V. Structural Insight into Iodide Uptake by AFm Phases. Environ. Sci. Technol. **2012**, 46 (7), 3874–3881. https://doi.org/10.1021/es204470e.

(6) Um, W.; Serne, R. J.; Krupka, K. M. Linearity and Reversibility of Iodide Adsorption on Sediments from Hanford, Washington under Water Saturated Conditions. Water Res. **2004**, 38 (8), 2009–2016. https://doi.org/10.1016/j.watres.2004.01.026.

(7) Coughtrey, P. J.; Thorne, M. C. Radionuclide Distribution and Transport in Terrestrial and Aquatic Ecosystems. A Critical Review of Data; 1983; Vol. 1.

(8) Whitehead, D. C. The Distribution and Transformations of Iodine in the Environment. Environ. Int. **1984**, 10 (4), 321–339. https://doi.org/10.1016/0160-4120(84)90139-9.

(9) Schwehr, K. A.; Santschi, P. H.; Kaplan, D. I.; Yeager, C. M.; Brinkmeyer, R. Organo-Iodine Formation in Soils and Aquifer Sediments at Ambient Concentrations. Environ. Sci. Technol. **2009**, 43 (19), 7258–7264. https://doi.org/10.1021/es900795k.

(10) Shimamoto, Y. S.; Takahashi, Y.; Terada, Y. Formation of Organic Iodine Supplied as Iodide in a Soil−Water System in Chiba, Japan. Environ. Sci. Technol. **2011**, 45 (6), 2086–2092. https://doi.org/10.1021/es1032162.

(11) Fuge, R.; Johnson, C. C. Iodine and Human Health, the Role of Environmental Geochemistry and Diet, a Review. Appl. Geochem. **2015**, 63, 282–302. https://doi.org/10.1016/j.apgeochem.2015.09.013.

(12) Patrick, L. Iodine: Deficiency and Therapeutic Considerations. Altern. Med. Rev. **2008**, 13 (2), 116–127.

(13) Audubert, F.; Carpena, J.; Lacout, J. L.; Tetard, F. Elaboration of an Iodine-Bearing Apatite Iodine Diffusion into a Pb3(VO4)2 Matrix. Solid State Ion. **1997**, 95 (1), 113–119. https://doi.org/10.1016/S0167-2738(96)00570-X.

(14) Garino, T. J.; Nenoff, T. M.; Krumhansl, J. L.; Rademacher, D. X. Low-Temperature Sintering Bi–Si–Zn-Oxide Glasses for Use in Either Glass Composite Materials or Core/Shell 129I Waste Forms. J. Am. Ceram. Soc. **2011**, 94 (8), 2412–2419. https://doi.org/10.1111/j.1551-2916.2011.04542.x.

(15) Krumhansl, J. L.; Nenoff, T. M. Hydrotalcite-like Layered Bismuth–Iodine–Oxides as Waste Forms. Applied Geochemistry **2011**, 26 (1), 57–64. https://doi.org/10.1016/j.apgeochem.2010.11.003.

(16) Sava, D. F.; Garino, T. J.; Nenoff, T. M. Iodine Confinement into Metal–Organic Frameworks (MOFs): Low-Temperature Sintering Glasses To Form Novel Glass Composite Material (GCM) Alternative Waste Forms. Ind. Eng. Chem. Res. **2012**, 51 (2), 614–620. https://doi.org/10.1021/ie200248g.

(17) Sava, D. F.; Rodriguez, M. A.; Chapman, K. W.; Chupas, P. J.; Greathouse, J. A.; Crozier, P. S.; Nenoff, T. M. Capture of Volatile Iodine, a Gaseous Fission Product, by Zeolitic Imidazolate

Framework-8. J. Am. Chem. Soc. **2011**, 133 (32), 12398–12401. https://doi.org/10.1021/ja204757x.
(18) Riley, B. J.; Vienna, J. D.; Strachan, D. M.; McCloy, J. S.; Jerden, J. L. Materials and Processes for the Effective Capture and Immobilization of Radioiodine: A Review. J. Nucl. Mater. **2016**, 470, 307–326. https://doi.org/10.1016/j.jnucmat.2015.11.038.
(19) Frankel, G. S.; Vienna, J. D.; Lian, J.; Scully, J. R.; Gin, S.; Ryan, J. V.; Wang, J.; Kim, S. H.; Windl, W.; Du, J. A Comparative Review of the Aqueous Corrosion of Glasses, Crystalline Ceramics, and Metals. npj Materials Degradation **2018**, 2 (1), 15. https://doi.org/10.1038/s41529-018-0037-2.
(20) Faucon, P.; Adenot, F.; Jacquinot, J. F.; Petit, J. C.; Cabrillac, R.; Jorda, M. Long-Term Behaviour of Cement Pastes Used for Nuclear Waste Disposal: Review of Physico-Chemical Mechanisms of Water Degradation. Cem. Concr. Res. **1998**, 28 (6), 847–857. https://doi.org/10.1016/S0008-8846(98)00053-2.
(21) Frankel, G. S.; Vienna, J.; Lian, J. WastePD, an Innovative Center on Materials Degradation. npj Mater. Degrad. **2017**, 1 (1), 5. https://doi.org/10.1038/s41529-017-0002-5.
(22) Chapman, N. A.; McKinley, I. G.; Smellie, J. a. T. The Potential of Natural Analogues in Assessing Systems for Deep Disposal of High-Level Radioactive Waste; EIR--545; Eidgenoessisches Inst. fuer Reaktorforschung: Sweden, 1984.
(23) Kato, H.; Kato, O.; Tanabe, H. Review of Immobilization Techniques of Radioactive Iodine for Geological Disposal. **2002**. https://doi.org/10.11484/JAERI-Conf-2002-004.
(24) Chapman, K. W.; Chupas, P. J.; Nenoff, T. M. Radioactive Iodine Capture in Silver-Containing Mordenites through Nanoscale Silver Iodide Formation. J. Am. Chem. Soc. **2010**, 132 (26), 8897–8899. https://doi.org/10.1021/ja103110y.
(25) Yao, T.; Lu, F.; Sun, H.; Wang, J.; Ewing, R. C.; Lian, J. Bulk Iodoapatite Ceramic Densified by Spark Plasma Sintering with Exceptional Thermal Stability. J. Am. Ceram. Soc. **2014**, 97 (8), 2409–2412. https://doi.org/10.1111/jace.13101.
(26) Maddrell, E.; Gandy, A.; Stennett, M. The Durability of Iodide Sodalite. Journal of Nuclear Materials **2014**, 449 (1), 168–172. https://doi.org/10.1016/j.jnucmat.2014.03.016.
(27) Chong, S.; Peterson, J. A.; Riley, B. J.; Tabada, D.; Wall, D.; Corkhill, C. L.; McCloy, J. S. Glass-Bonded Iodosodalite Waste Form for Immobilization of 129I. J. Nucl. Mater. **2018**, 504, 109–121. https://doi.org/10.1016/j.jnucmat.2018.03.033.
(28) Le Gallet, S.; Campayo, L.; Courtois, E.; Hoffmann, S.; Grin, Yu.; Bernard, F.; Bart, F. Spark Plasma Sintering of Iodine-Bearing Apatite. J. Nucl. Mater. **2010**, 400 (3), 251–256. https://doi.org/10.1016/j.jnucmat.2010.03.011.
(29) Zhang, Z.; Heath, A.; T. Valsaraj, K.; L. Ebert, W.; Yao, T.; Lian, J.; Wang, J. Mechanism of Iodine Release from Iodoapatite in Aqueous Solution. RSC Adv. **2018**, 8 (8), 3951–3957. https://doi.org/10.1039/C7RA11049A.
(30) Gauthier-Lafaye, F. 2 Billion Year Old Natural Analogs for Nuclear Waste Disposal: The Natural Nuclear Fission Reactors in Gabon (Africa). C. R. Phys. **2002**, 3 (7), 839–849. https://doi.org/10.1016/S1631-0705(02)01351-8.
(31) Uno, M.; Shinohara, M.; Kurosaki, K.; Yamanaka, S. Some Properties of a Lead Vanado-Iodoapatite Pb10(VO4)6I2. J. Nucl. Mater. **2001**, 294 (1), 119–122. https://doi.org/10.1016/S0022-3115(01)00462-7.
(32) National Research Council. Scho; 2011. https://doi.org/10.17226/13100.
(33) Guy, C.; Audubert, F.; Lartigue, J.-E.; Latrille, C.; Advocat, T.; Fillet, C. New Conditionings for Separated Long-Lived Radionuclides. C. R. Phys. **2002**, 3 (7), 827–837. https://doi.org/10.1016/S1631-0705(02)01377-4.

(34) Zhang, M.; Maddrell, E. R.; Abraitis, P. K.; Salje, E. K. H. Impact of Leach on Lead Vanado-Iodoapatite [Pb5(VO4)3I]: An Infrared and Raman Spectroscopic Study. Mater. Sci. Eng. B **2007**, 137 (1), 149–155. https://doi.org/10.1016/j.mseb.2006.11.003.
(35) Coulon, A.; Grandjean, A.; Laurencin, D.; Jollivet, P.; Rossignol, S.; Campayo, L. Durability Testing of an Iodate-Substituted Hydroxyapatite Designed for the Conditioning of 129I. J. Nucl. Mater. **2017**, 484, 324–331. https://doi.org/10.1016/j.jnucmat.2016.10.047.
(36) ASTM C1220-17, Standard Test Method for Static Leaching of Monolithic Waste Forms for Disposal of Radioactive Waste; ASTM International: West Conshohocken, PA, 2017.
(37) Zhang, Z.; Ebert, W. L.; Yao, T.; Lian, J.; Valsaraj, K. T.; Wang, J. Chemical Durability and Dissolution Kinetics of Iodoapatite in Aqueous Solutions. ACS Earth Space Chem. **2019**, 3 (3), 452-462. https://doi.org/10.1021/acsearthspacechem.8b00162.
(38) Zhu, Y.; Zhang, X.; Chen, Y.; Xie, Q.; Lan, J.; Qian, M.; He, N. A Comparative Study on the Dissolution and Solubility of Hydroxylapatite and Fluorapatite at 25°C and 45°C. Chem. Geol. **2009**, 268 (1), 89–96. https://doi.org/10.1016/j.chemgeo.2009.07.014.
(39) Cazalbou, S.; Eichert, D.; Ranz, X.; Drouet, C.; Combes, C.; Harmand, M. F.; Rey, C. Ion Exchanges in Apatites for Biomedical Application. J. Mater. Sci. Mater. Med. **2005**, 16 (5), 405–409. https://doi.org/10.1007/s10856-005-6979-2.
(40) Brenan, J. Kinetics of Fluorine, Chlorine and Hydroxyl Exchange in Fluorapatite. Chem. Geol. **1993**, 110 (1), 195–210. https://doi.org/10.1016/0009-2541(93)90254-G.
(41) Dorozhkin, S. V. A Review on the Dissolution Models of Calcium Apatites. Prog. Cryst. Growth Charact. **2002**, 44 (1), 45–61. https://doi.org/10.1016/S0960-8974(02)00004-9.
(42) Petříček, V.; Dušek, M.; Palatinus, L. Crystallographic Computing System JANA2006: General Features. Z. Kristallogr. Cryst. Mater. **2014**, 229 (5), 345–352. https://doi.org/10.1515/zkri-2014-1737.
(43) Audubert, F.; Savariault, J.-M.; Lacout, J.-L. Pentalead Tris(Vanadate) Iodide, a Defect Vanadinite-Type Compound. Acta Crystallogr. C **1999**, 55 (3), 271–273. https://doi.org/10.1107/S0108270198005034.
(44) Ślósarczyk, A.; Paszkiewicz, Z.; Paluszkiewicz, C. FTIR and XRD Evaluation of Carbonated Hydroxyapatite Powders Synthesized by Wet Methods. J. Mol. Struct. **2005**, 744–747, 657–661. https://doi.org/10.1016/j.molstruc.2004.11.078.
(45) Merry, J. C.; Gibson, I. R.; Best, S. M.; Bonfield, W. Synthesis and Characterization of Carbonate Hydroxyapatite. J. Mater. Sci. Mater. Med. **1998**, 9 (12), 779–783. https://doi.org/10.1023/A:1008975507498.
(46) Roobottom, H. K.; Jenkins, H. D. B.; Passmore, J.; Glasser, L. Thermochemical Radii of Complex Ions. J. Chem. Educ. **1999**, 76 (11), 1570. https://doi.org/10.1021/ed076p1570.
(47) Guidry, M. W.; Mackenzie, F. T. Experimental Study of Igneous and Sedimentary Apatite Dissolution: Control of PH, Distance from Equilibrium, and Temperature on Dissolution Rates. Geochim. Cosmochim. Acta **2003**, 67 (16), 2949–2963. https://doi.org/10.1016/S0016-7037(03)00265-5.
(48) Cao, C.; Chong, S.; Thirion, L.; C. Mauro, J.; S. McCloy, J.; Goel, A. Wet Chemical Synthesis of Apatite-Based Waste Forms – A Novel Room Temperature Method for the Immobilization of Radioactive Iodine. J. Mater. Chem. C **2017**, 5 (27), 14331–14342. https://doi.org/10.1039/C7TA00230K.
(49) Campayo, L.; Audubert, F.; Lartigue, J.-E.; Courtois-Manara, E.; Gallet, S. L.; Bernard, F.; Lemesle, T.; Mear, F. O.; Montagne, L.; Coulon, A.; et al. French Studies on the Development of Potential Conditioning Matrices for Iodine 129. Mater. Res. Soc. Symp. Proc. **2015**, 1744, 15–20. https://doi.org/10.1557/opl.2015.309.

(50) Zapanta-Legeros, R. Effect of Carbonate on the Lattice Parameters of Apatite. Nature **1965**, 206 (4982), 403. https://doi.org/10.1038/206403a0.
(51) White, T. J.; Dong, Z. L. Structural Derivation and Crystal Chemistry of Apatites. Acta Cryst. B **2003**, 59 (1), 1–16. https://doi.org/10.1107/S0108768102019894.
(52) Fleet, M. E.; Liu, X. Coupled Substitution of Type A and B Carbonate in Sodium-Bearing Apatite. Biomaterials **2007**, 28 (6), 916–926. https://doi.org/10.1016/j.biomaterials.2006.11.003.
(53) Landi, E.; Tampieri, A.; Celotti, G.; Vichi, L.; Sandri, M. Influence of Synthesis and Sintering Parameters on the Characteristics of Carbonate Apatite. Biomaterials **2004**, 25 (10), 1763–1770. https://doi.org/10.1016/j.biomaterials.2003.08.026.

614 **Graphical abstract**

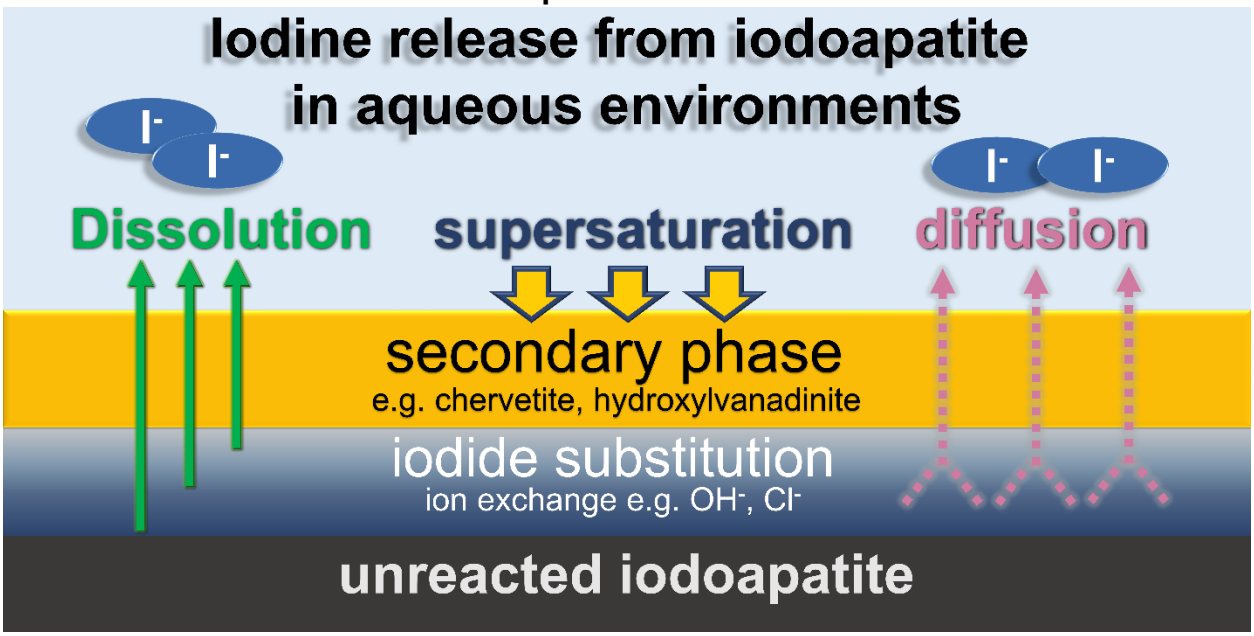

615

616

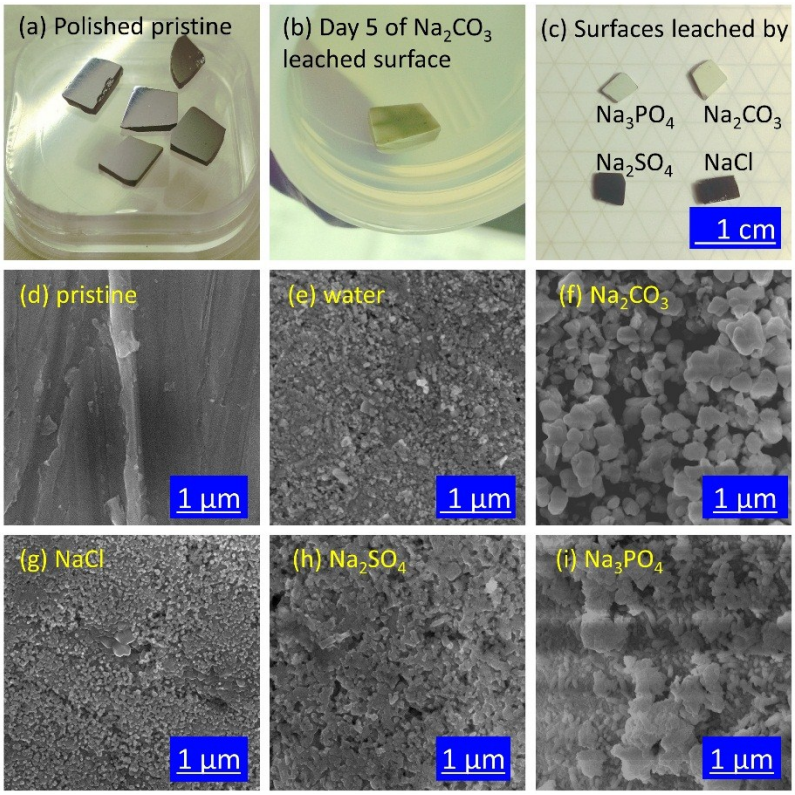

Fig. 1.(a) Polished pristine iodoapatite samples before test, (b) iodoapatite leached surface during the 5th replacement of Na_2CO_3 solution, (c) surface leached by at the end of 14-day leaching tests, SEM images of (a) a polished pristine iodoapatite and the samples leached by (b) deionized water, (c) 0.1 mol/L Na_2CO_3, (d) 0.1 mol/L NaCl, (e) 0.1 mol/L Na_2SO_4, and (f) 0.1 mol/L Na_3PO_4.

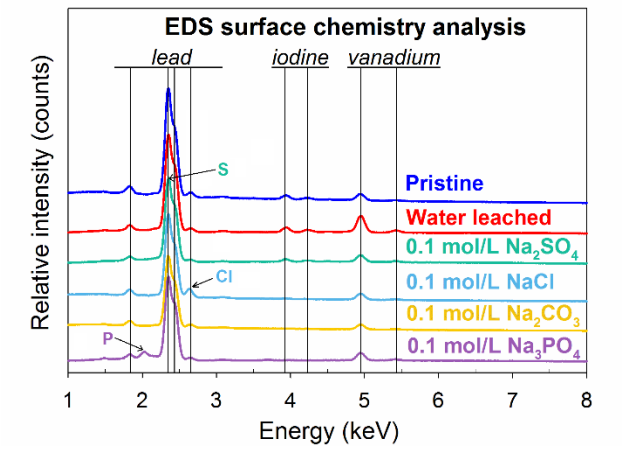

624

625 Fig. 2. EDS spectra of a pristine iodoapatite and the samples leached by deionized
626 water, 0.1 mol/L NaCl, 0.1 mol/L Na_2CO_3, 0.1 mol/L Na_3PO_4, and 0.1 mol/L Na_2SO_4
627 solutions.

628

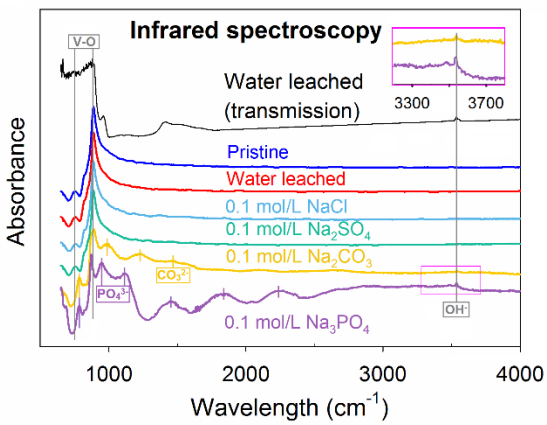

629

630 Fig. 3. Infrared spectroscopy of pristine iodoapatite and leached samples by deionized
631 water, NaCl, Na_2SO_4, Na_2CO_3, and Na_3PO_4 solutions.

632

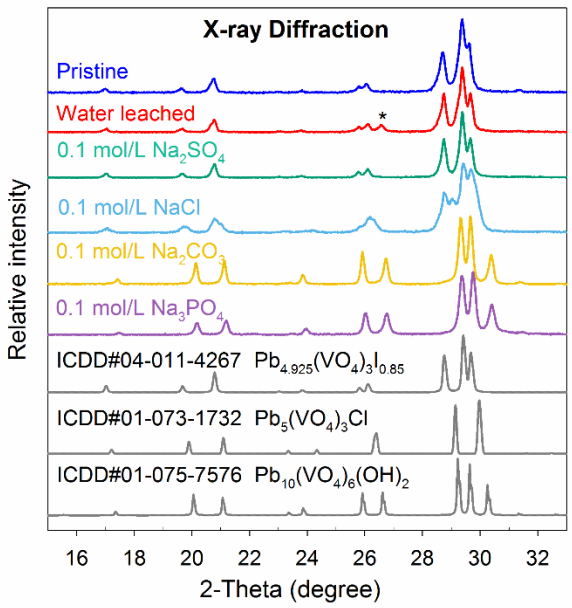

633

634 Fig. 4. XRD patterns of a pristine iodoapatite and the samples leached by deionized
635 water, 0.1 mol/L Na_2SO_4, 0.1 mol/L NaCl, 0.1 mol/L Na_2CO_3, and 0.1 mol/L Na_3PO_4. In
636 addition, standard XRD spectra of iodoapatite, vanadinite, and hydroxylvanadinite are
637 listed for comparison. * denotes the graphite impurity introduced during sample
638 synthesis.[25]

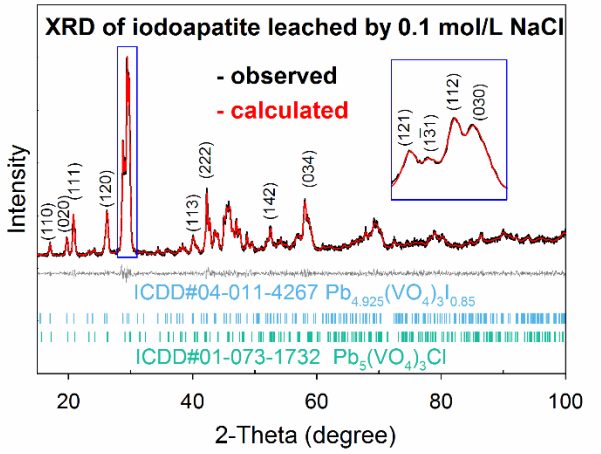

639

640 Fig. 5. XRD phase analysis of the iodoapatite sample surface leached by 0.1
641 mol/L NaCl solution. Two phases were identified: iodoapatite and vanadinite.

642

643

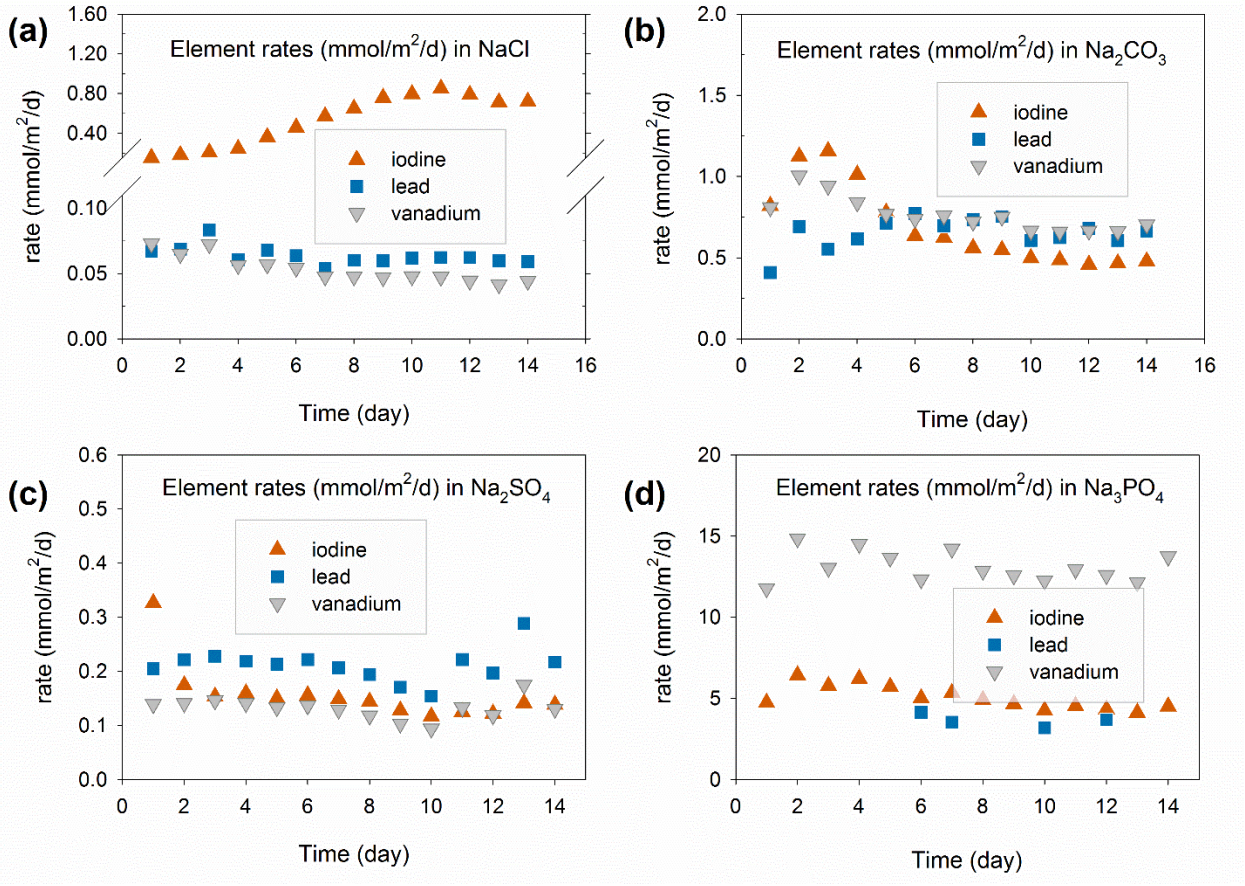

644

645 Fig. 6. Solution analysis of collected leachates from 14 days semi-dynamic leach tests
646 on iodoapatite samples in (a) 0.1 mol/L NaCl, (b) 0.1 mol/L Na_2CO_3, (c) 0.1 mol/L
647 Na_2SO_4, and (d) 0.1 mol/L Na_3PO_4.

648

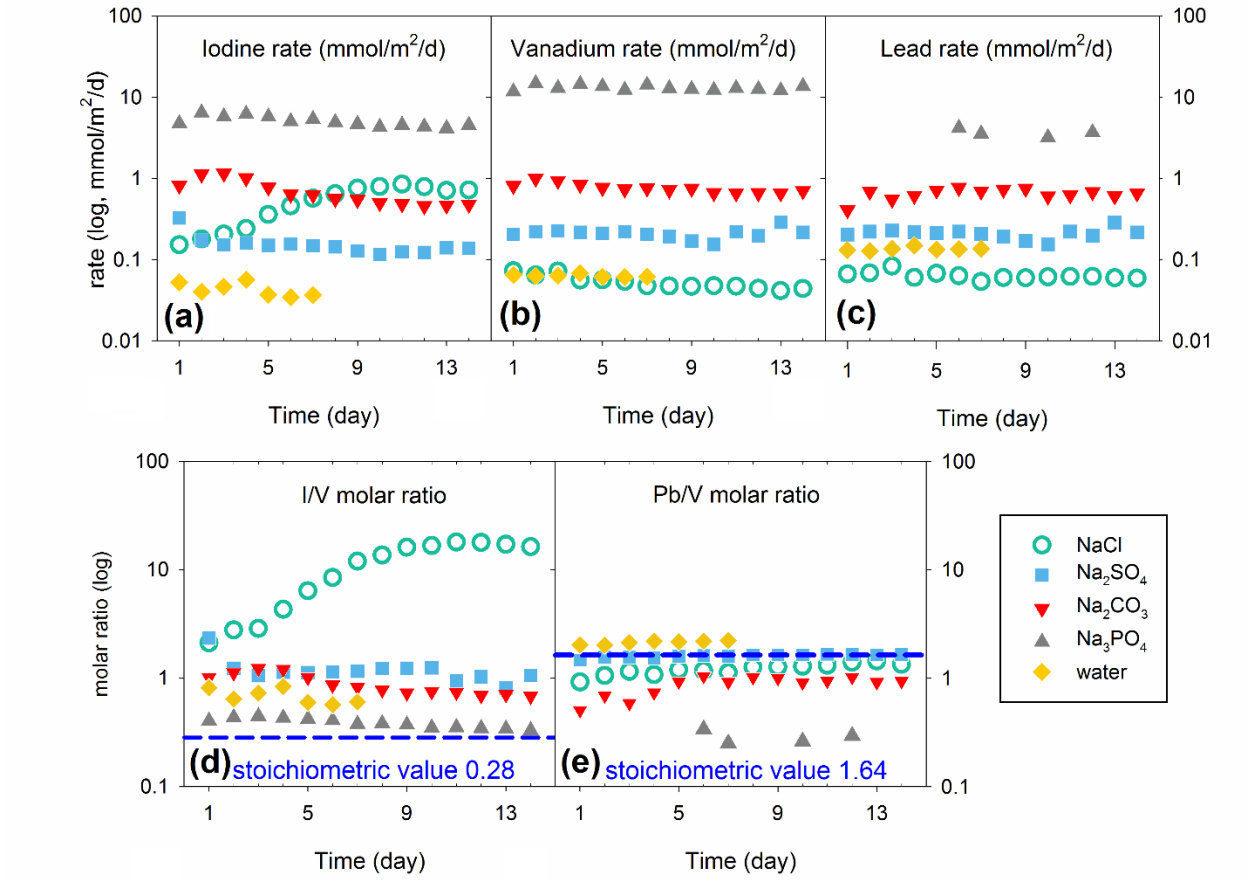

649

650 Fig. 7. Comparison of element release rate of iodine (a), vanadium (b), and lead (c) in
651 the leachate solutions from different leach tests. Molar ratios of Pb/V (d) and I/V (e) in
652 leachate solutions from leach tests in NaCl, Na_2SO_4, Na_2CO_3, Na_3PO_4, and deionized
653 water.

654

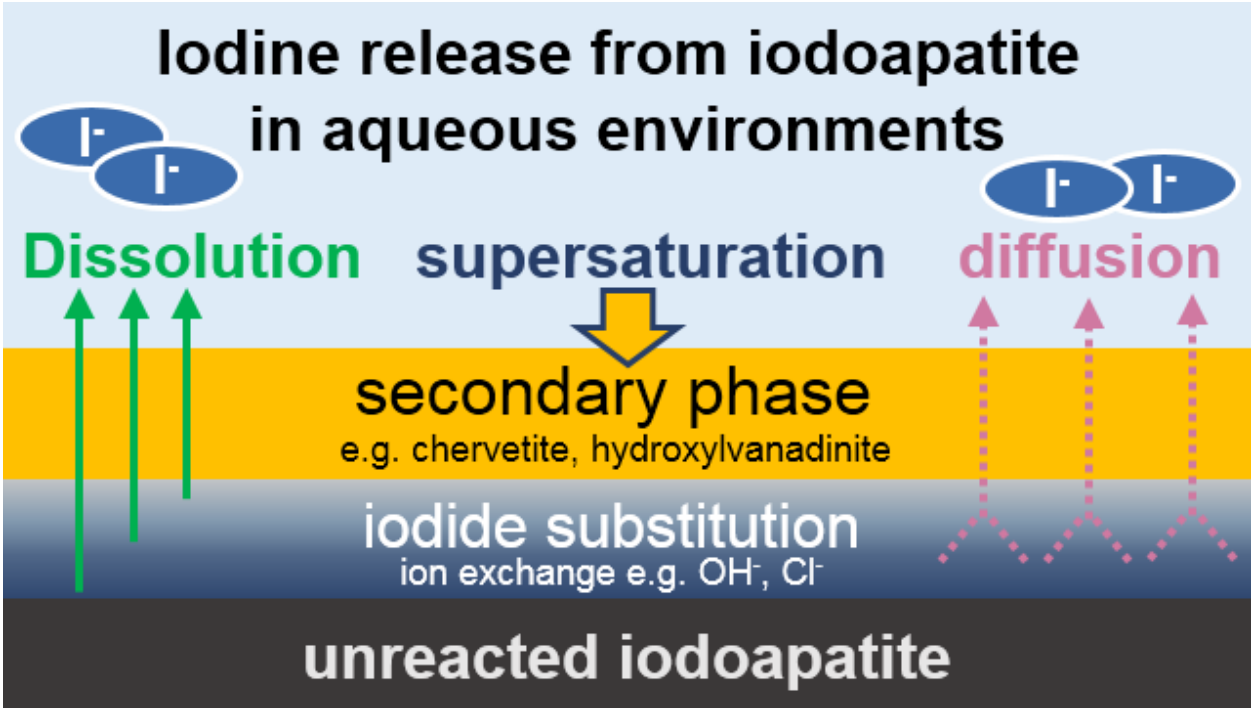

Fig. 8. Schematic diagram illustrates major processes that control the iodine release from iodoapatite in aqueous environments

Table. 1 Crystallographic parameters based on the XRD refinements by Le Bail algorithm.

Leach test condition	Refined parameters				
	a, b (a=b, Å)	c (Å)	GoF	R_p (%)	R_{wp} (%)
Pristine	10.4420 (3)	7.4756 (3)	1.32	5.16	6.53
Water	10.4325 (3)	7.4864 (3)	1.63	6.04	7.73
0.1 mol/L Na_2SO_4	10.4336 (2)	7.4837 (2)	1.39	4.60	5.93
0.1 mol/L Na_2CO_3	10.1923 (2)	7.4656 (2)	1.65	4.85	6.44
0.1 mol/L Na_3PO_4	10.1984 (2)	7.4449 (2)	1.43	4.74	6.23
0.1 mol/L NaCl (2 phases)	10.4443 (6) 10.3536 (8)	7.4796 (5) 7.3735(8)	1.17	4.12	5.28
$Pb_{4.925}(VO_4)_3I_{0.85}$ [ICDD#04-011-4267]	10.422	7.467	**Crystal system: hexagonal**		
$Pb_5(VO_4)_3(OH)$ [ICDD#01-075-7576]	10.2242	7.4537	**Space group: P63/m #176;**		
$Pb_5(VO_4)_3Cl$ [ICDD#01-073-1732]	10.31	7.34	**α=90° β=90° γ=120°**		

662 Table 2. Solution chemistry at equilibrium state calculated by Visual MINTEQ under
663 90 °C.

mol/L 90 °C	Deionized water	0.1 mol/L NaCl	0.1 mol/L Na_2SO_4	0.1 mol/L Na_2CO_3	0.1 mol/L Na_3PO_4
pH (unitless)	6.1	6.1	6.2	10.3	10.9
Ionic strength	2.04×10^{-6}	0.098	0.26	0.25	0.29
Major cation	**H^+**	**Na^+**	**Na^+**	**Na^+**	**Na^+**
Concentration	6.52×10^{-7}	0.098	0.18	0.18	0.22
Activity	6.51×10^{-7}	0.074	0.13	0.13	0.15
Activity coefficient	1.00	0.76	0.72	0.72	0.68
Major anion	**OH^-**	**Cl^-**	**SO_4^{2-}**	**CO_3^{2-}**	**PO_4^{3-}**
Concentration	8.72×10^{-7}	0.098	0.079	0.069	0.012
Activity	8.70×10^{-7}	0.074	0.02	0.017	0.00049
Activity coefficient	1.00	0.76	0.25	0.24	0.041

664